Model Geometry. The geometry of the simulation is as follows. Excavations representing the AOD, Cross Drift, Heated Drift, and Plate Loading Niche were excavated from a simulated block of rock with dimensions 110 m × 55 m × 50 m. Then fractures listed in Table 5 were introduced. These fractures are allowed to extend to the edges of the model domain. The model domain with fractures included is shown in Figure 126. Excavations are shown in Figure 127.

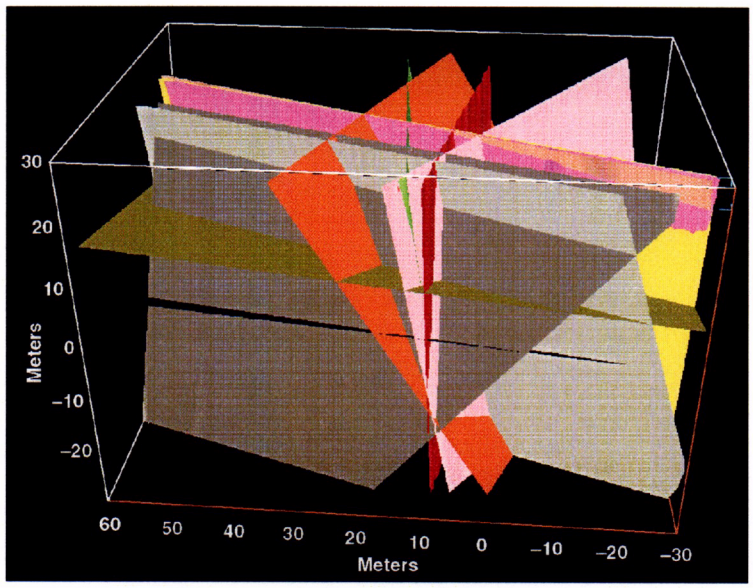

Figure 126. Model Domain with Fractures Included, Used for Basecase Simulation.

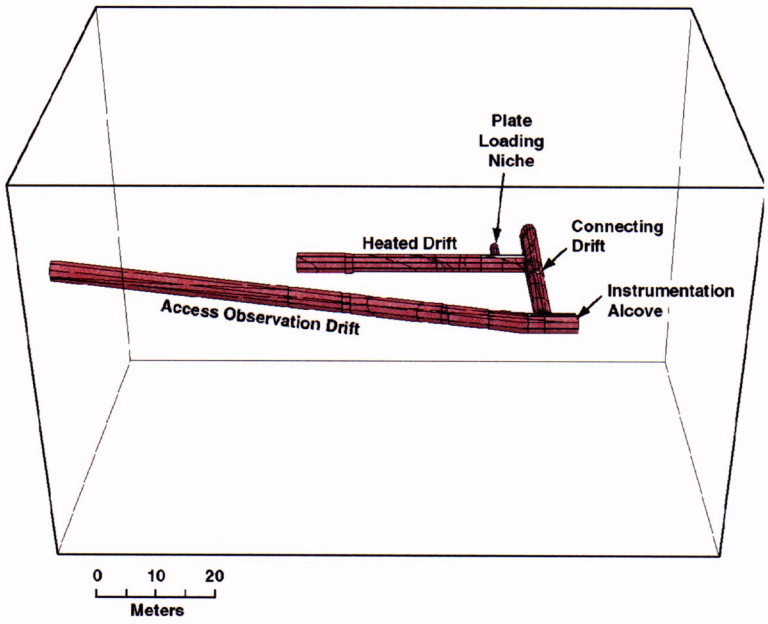

Figure 127. Excavations of Drifts and Niches Associated with the DST from the Model Domain.

C-80

Boundary Conditions. Boundary conditions were applied to the simulated rock mass as follows. The base of the model was considered to be a roller boundary so that no vertical displacement was allowed. However, horizontal displacements were allowed.

The vertical sides and top of the rock mass were considered stress boundaries, and an in situ stress condition was applied with a vertical stress of 9.7 MPa and a horizontal stress of 4.85 MPa (Schelling 1989). Stress gradients were 0.023 MPa per meter of depth for vertical stresses and 0.0115 MPa per meter of depth for horizontal stresses. The stress boundary is considered appropriate as rock surrounding the DST is at ambient conditions.

Rock Properties. Both the DST and LBT are sited in the middle nonlithophysal unit of the Topopah Spring Tuff. Input parameters for the TM emplacement drift base case are provided in Table 6 and are the same as those used for the emplacement drift analysis presented in CRWMS M&O 2001. Calculated or assumed parameters are listed in Table 7. Bulk and shear modulus can be calculated from the elastic modulus (E) and Poisson's ratio (ν) as

$$K = E/(3(1-(2\nu))) \quad \text{and} \quad G = E/(2(1+\nu))$$

(Jaeger and Cook 1979), and values are given in Table 7. The input values for joint normal stiffness and joint shear stiffness assume a joint spacing of 1 m and were calculated with a relationship given in the 3DEC User's Guide (Itasca 1998, Section 3, p. 94). The joint normal stiffness calculation used an intact rock elastic modulus of 33.03 GPa (DTN: MO9911SEPGRP34.000, Table 8) and a rock mass elastic modulus of 24.71 GPa (DTN: MO9911SEPGRP34.000, Table 10). Shear moduli for the joint shear stiffness calculation were obtained from the above elastic moduli and a Poisson's ratio of 0.21 (DTN: MO9911SEPGRP34.000, Table 11). The other input parameter values were taken directly from the Technical Data Management System. The input parameters are considered appropriate because they are derived from field and laboratory measurements of the host rock physical properties, or are based on EDA II design parameters.

Table 6. Input Parameters and Data Tracking Numbers

Item No.	Description	Value	Units	Data Tracking Number
	Matrix Properties			
1	Dry Bulk Density	2270	kg/m^3	MO0003SEPDRDDA.000
2	Intact Rock Elasticity Modulus	33.03	GPa	MO9911SEPGRP34.000
3	Rock Mass Elasticity Modulus	24.71	GPa	MO9911SEPGRP34.000
4	Poisson's Ratio	0.21	none	MO9911SEPGRP34.000
	Joint Properties			
5	Joint Friction	41	deg	MO0010RDDAAMRR.002
6	Joint Cohesion	0.09	MPa	MO9911SEPGRP34.000
	Thermal Properties			
7	Thermal Conductivity	2.33	W/m-K	MO9911SEPGRP34.000
8	Thermal Expansion Coefficient	9.73E-6	deg C^{-1}	SNL22100196001.001
	Input Temperatures			
9	Input Temperatures	various	deg C	LL000114004242.090

Table 7. Calculated or Assumed Model Parameters

Description	Value	Units
Matrix Properties		
Rock Mass Bulk Modulus	14.2	GPa
Rock Mass Shear Modulus	10.2	GPa
Joint Properties		
Joint Tensile Strength	0	MPa
Joint Normal Stiffness	98.1	MPa/mm
Joint Shear Stiffness	40.5	MPa/mm
Joint Dilation Angle	29	deg
Initial Joint Aperture	0.098	mm
Boundary and In Situ Stresses		
In Situ Stress (280 m depth)	5.54	MPa
Vertical Stress Gradient	0.021	MPa/m

Results for Drift Scale Test

This section presents results of the model predictions of displacement for MPBX systems used in the DST, and compares the predicted displacements with those observed during the first 545 days of heating in the DST. For this analysis, comparisons are made for MPBX data collected for 10 of the 17 MPBX boreholes in the DST. The boreholes and anchors used are listed in Table 8.

Moreover, in the Qualitative Results discussion below, model predictions at a series of times are compared with observations. This is done for the deepest anchor in the MPBX boreholes listed in Table 8. The deepest anchor was chosen as it best represents the rock mass behavior. Note that for boreholes 42 and 43 anchor 1 is the deepest, while for the remainder of the boreholes anchor 6 is the deepest, i.e., farthest from the borehole collar.

Table 8. List of MPBX Anchors Simulated for DST

Hole	Anchor No.					
42	1	2	3	4	5	6
43	1	2	3	4	5	6
81	1	2	3	4	5	6
82	1	2	3	4	5	6
147	1	2	3	4		
148	1	2	3	4		
149			3	4		
150		2		4		
156				4		
180				4		

Qualitative Results. ***Simulation of Mine-by***—Prior to the excavation of the HD three boreholes were drilled from the AOD perpendicular to the planned location of the HD. These boreholes (42, 43, and 44) were instrumented with MPBX systems and deformations were recorded during the excavation of the HD. The borehole response due to the excavation was simulated using the DSDE model, and can be used to calibrate the bulk and shear moduli of the rock mass in the simulation.

The excavation of the HD was simulated by excavating the entire length of the HD at one time. Thus the time history of the HD excavation was not simulated, but the effect of the excavation on the rock in boreholes 42 and 43 was determined. Borehole 44 was not used in this analysis as the data for this borehole were judged to be of poor quality.

The deformation of the deepest anchors in boreholes 42 and 43 was simulated and the resulting total deformation is listed for the simulation in Table 9 along with total deformation as measured by the MPBX systems. The total deformation is shown graphically for boreholes 42 and 43 in Figure 128. This figure shows that the prediction overestimates the observed deformation by 45% in borehole 42, and by 32% in borehole 43. Thus both estimates are within an order of magnitude of the observations.

Table 9. Deformation Due to Mine-by of HD

Borehole	Anchor 6 max (mm)	Predicted deformation (mm)
42	2.4	3.5
43	3.1	4.1

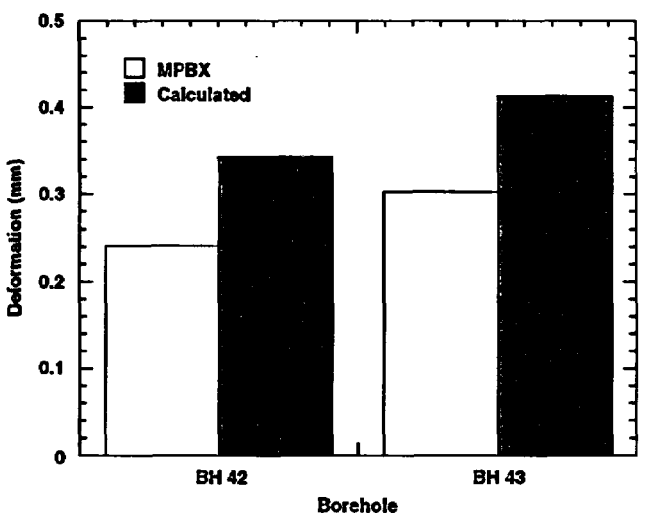

Figure 128. Total Deformation for Boreholes 42 and 43 During Mine-by, Prior to Heating.

Heating Phase of DST—

Boreholes 42 and 43: These boreholes extend from AOD toward the HD and were used for mine-by as discussed above. Observed and predicted deformations for these boreholes after heating started are shown in Figures 129 and 130. Figure 129 shows that for the first 250 days, the basecase model simulated deformation very well for Borehole 42. After 300 days, the observed deformation rate is higher than predicted, and the fit is not as good.

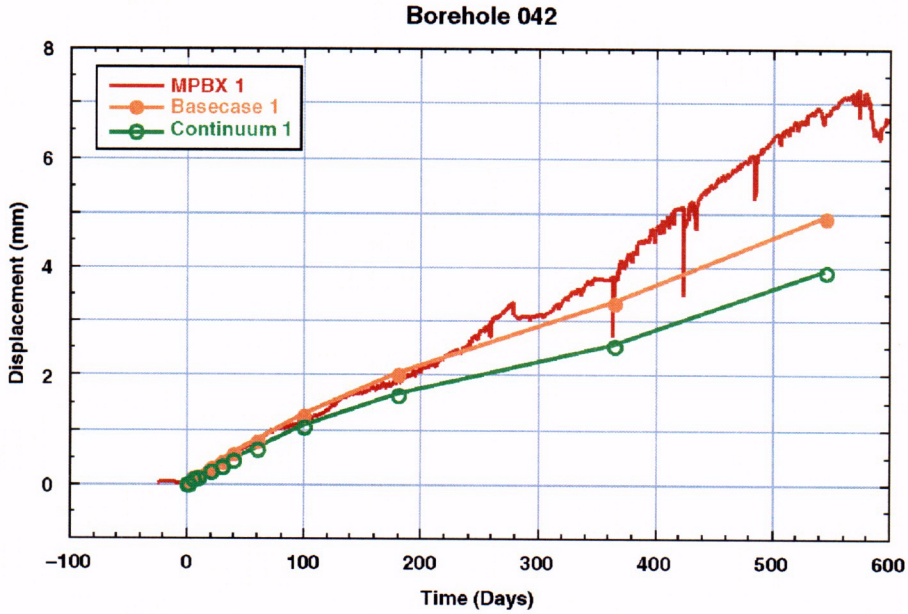

Figure 129. Observed and Predicted Deformation for BH 42.

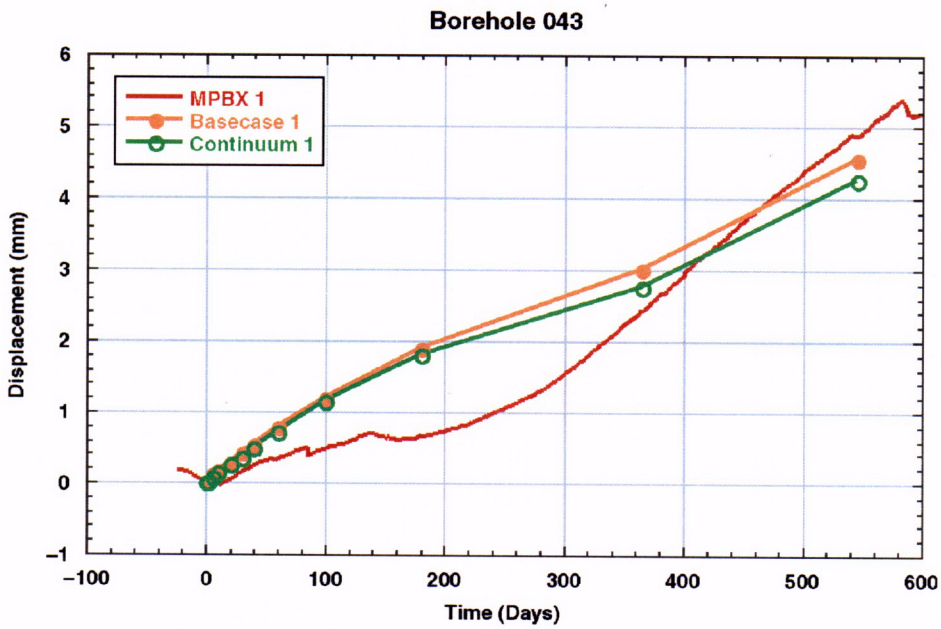

Figure 130. Observed and Predicted Deformation for BH 43.

C-81

At 240 days the basecase model matches the prediction to better than 10%, but at 545 days the basecase model predicts 70% of the observed value. The continuum model underpredicts the deformation throughout the 545-day period and, at 545 days, the value predicted by the continuum model is 57% of the observed value.

Observed and predicted behavior for BH 43 is shown in Figure 130. This borehole is roughly parallel to BH 42 (see Figure 123) and, as expected, the predicted deformations are similar to those predicted for BH 42, with the basecase model predicting more deformation than the continuum model.

However, the observed deformation for BH 43 anchor 1 shows a much different trend than deformation observed for borehole 42, with a low rate of deformation for the first 200 days of heating. After 200 days, the deformation rate increases dramatically to slightly less than the 0.016 mm/day observed for BH 42 after approximately 300 days.

Boreholes 81 and 82: Figures 131 and 132 show results for boreholes 81 and 82. These boreholes are parallel to the HD, 3.4 m above the center of the wing heaters, and are collared in the connecting drift. These figures show that both the basecase and the continuum models substantially underpredict the observed deformation for Anchor 6 in each of these boreholes.

The data show very little movement for the first 20 days, followed by increasing deformation (expansion), with boreholes 81 and 82 showing 5 and 6 mm of expansion, respectively, by 545 days of heating. In contrast, the predictions show negative deformation (compression) for the first 80 days, followed by expansion, but the predicted rate of expansion is much slower than that observed.

The observations and model predictions follow the same general trend between 80 and 400 days, during which both observed and predicted displacements rise at a diminishing rate. After 400 days, the observed displacements rise at an increasing rate, a feature which is not matched by the model. The total predicted deformation of approximately 1 mm is a factor of 6 lower than the 6 mm observed.

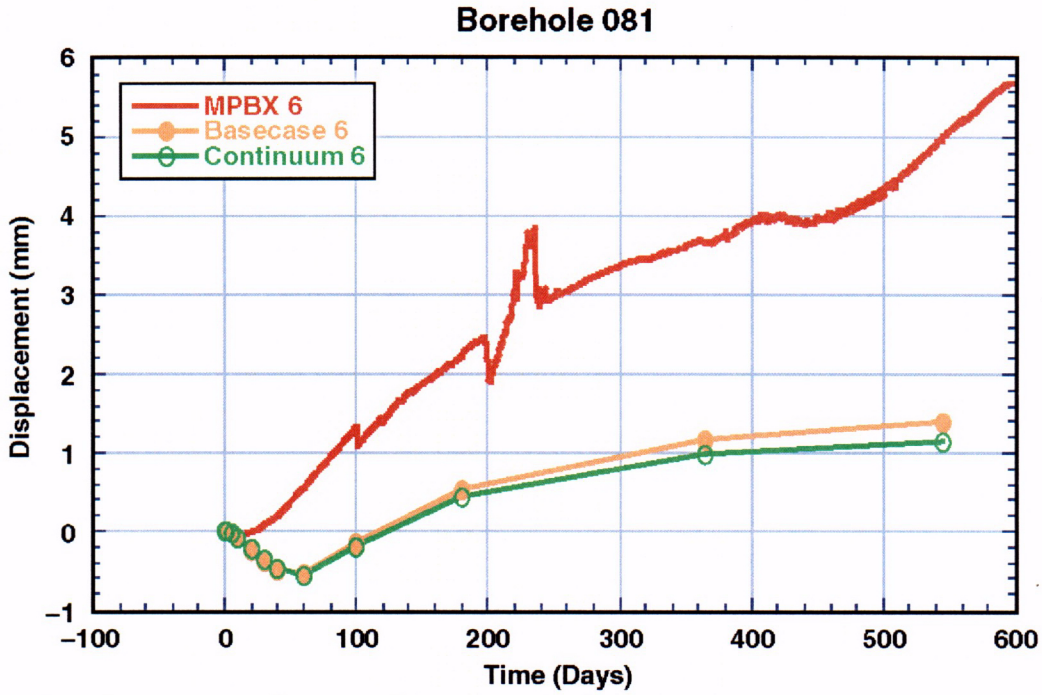

Figure 131. Observed and Predicted Deformation for BH 81.

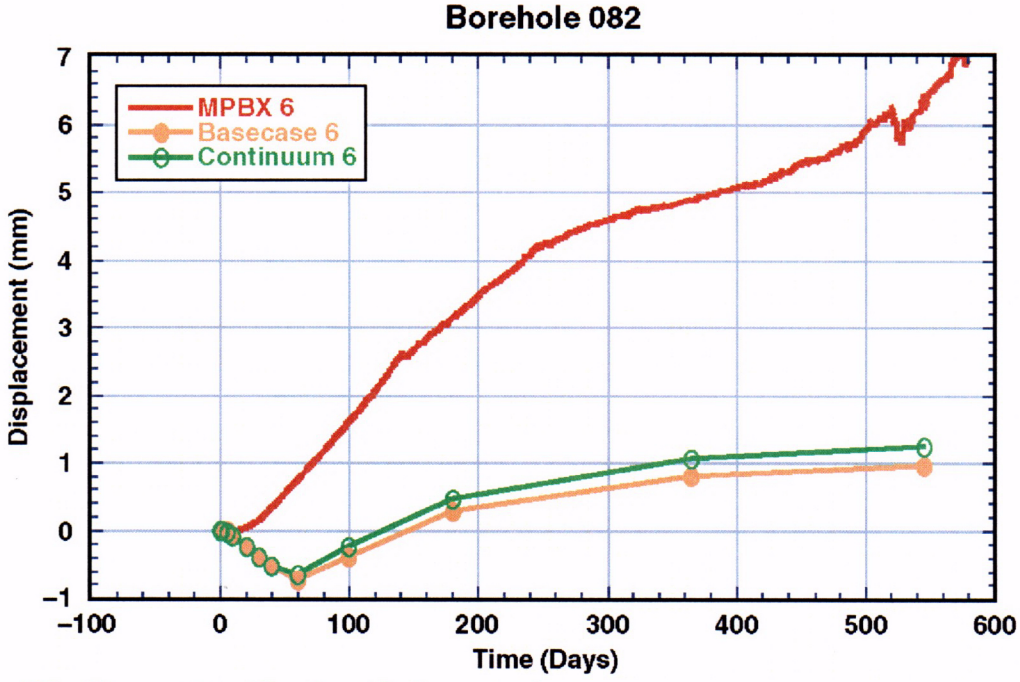

Figure 132. Observed and Predicted Deformation for BH 82.

C-82

Boreholes 147, 148, and 149: These boreholes are located in the crown of the HD, approximately 13 m from the bulkhead, and form along with BH 150 the first fan of three MPBX boreholes in the HD. The observed and predicted deformations for boreholes 147, 148, and 149 Anchor 4 are shown in Figures 133, 134, and 135.

Results for BH 147 (Figure 133) show that observed deformation begins immediately upon start of heating, while the predicted deformation doesn't begin until 40–50 days after heating. After 50 days the predicted slope is very similar to observation, and overall magnitude at 545 days is 5 mm for prediction vs. approximately 5.5 mm for observation. Thus the predicted value is 90% of the observed value. The basecase model predicts larger magnitude of deformation and starts somewhat sooner than the continuum model. Note that the sharp drops in deformation are interpreted to be associated with temperature changes in the borehole and not actual rock movements.

Predicted and observed deformations for BH 148 are shown in Figure 134. This borehole is angled toward the AOD. This figure shows that the observed displacement increases much more quickly after the start of heating than does the predicted displacement, but the difference is not as great as observed in BH 147.

A change in slope occurs at approximately 20–30 days, after which the slope is linear until approximately 250 days, when the rate of displacement decreases somewhat. The simulated deformation shows a lag in initial response similar to that predicted for BH 147. After approximately 60 days the slope of the basecase model matches the observation very well, while the expansion rate for the continuum model is too high. At 400 days the basecase model matches the observed value almost exactly.

Predicted and observed deformations for BH 149 are shown in Figure 135. This figure shows that the basecase model predicts behavior very well. This borehole is vertical in the crown (see Figure 123).

In initial behavior, the rock deforms during the first 10 days, while the predicted deformation does not start until after day 20. Agreement with data at 545 days is excellent, within 5%. The basecase model fits somewhat better than the continuum model

Examination of the three boreholes (147, 148, 149) as a group shows that deformation for BH 147 is greater than for BH 148 and 149. That is, at 400 days, boreholes 147, 148, and 149 show 4.4, 3.4, and 3.6 mm of displacement, respectively. This indicates that rock on the side away from the AOD is deforming more than the rock between the HD and the AOD. The basecase model predicts 3.6, 3.4, and 3.4 mm, respectively, while the continuum model predicts 3.4, 3.8, and 3.8 mm, respectively, for these boreholes at 400 days. Thus, the basecase model correctly predicts the trend of the measurement, as it indicates larger deformation for BH 147, and equal deformation for boreholes 148 and 149. The continuum model does not capture this behavior as well.

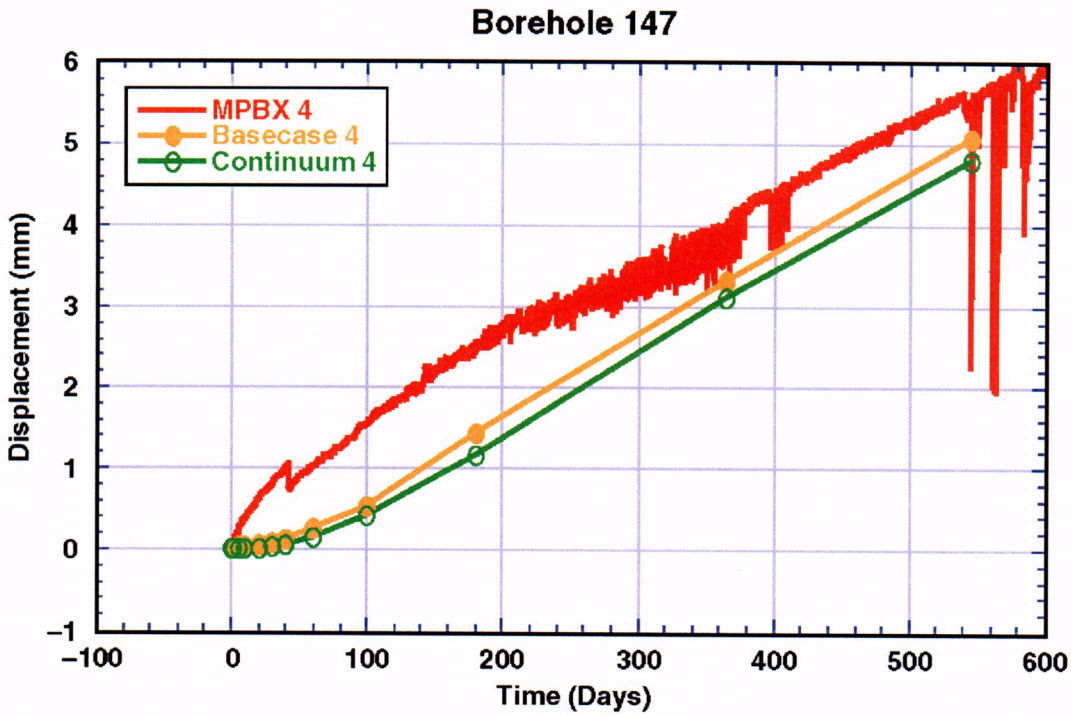

Figure 133. Observed and Predicted Deformation for BH 147.

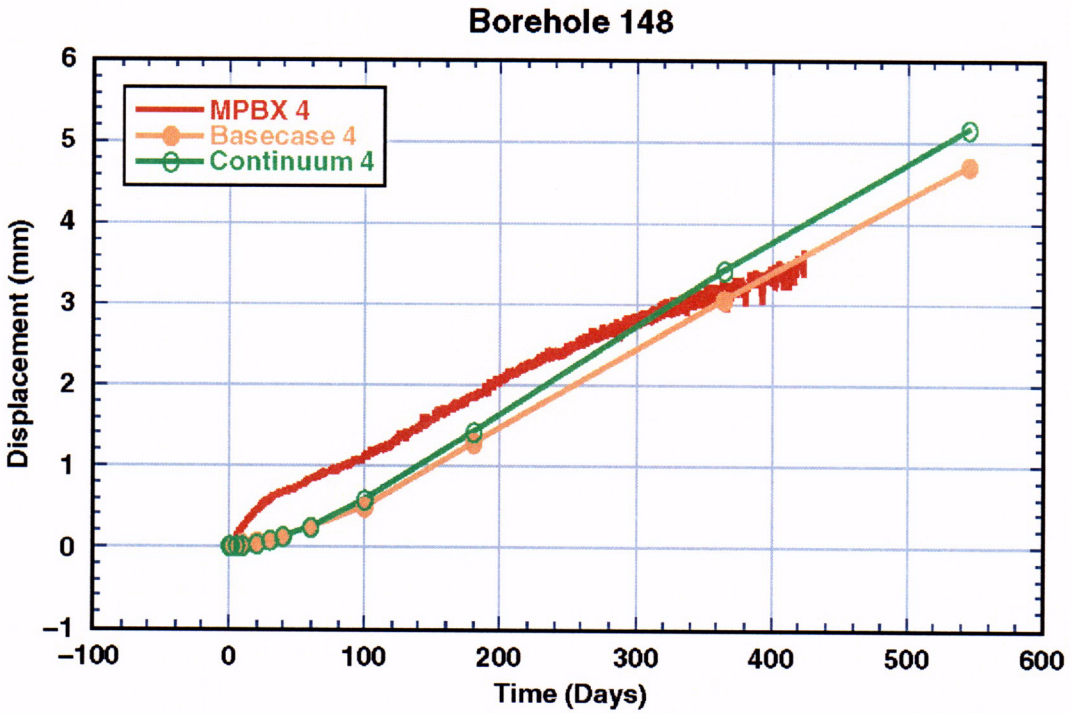

Figure 134. Observed and Predicted Deformation for BH 148.

C-83

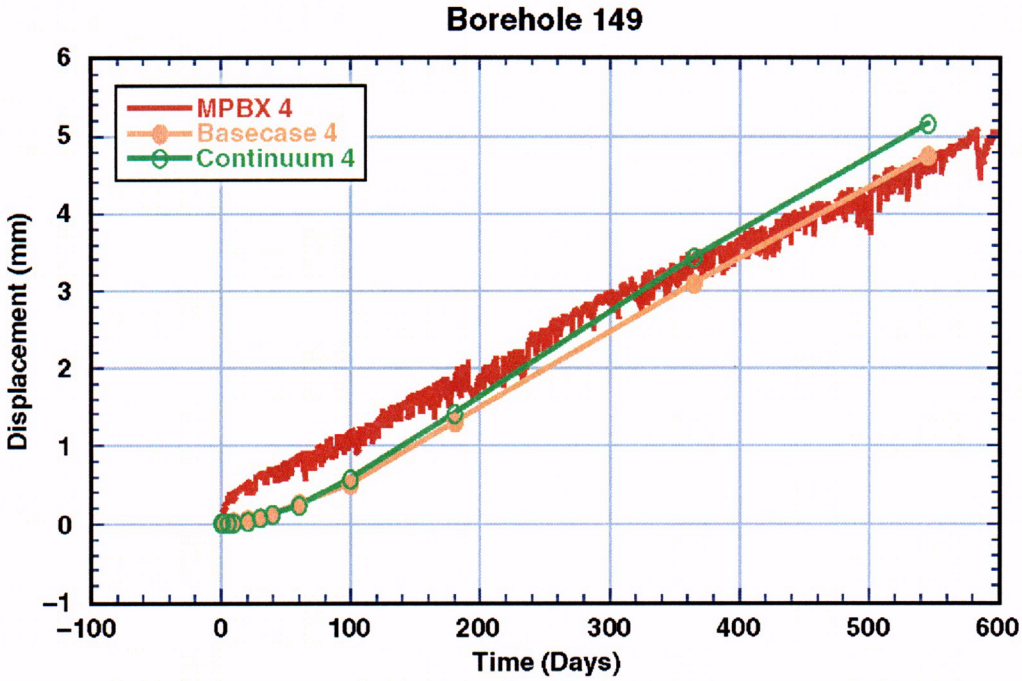

Figure 135. Observed and Predicted Deformation for BH 149.

Borehole 150: Results for BH 150 are shown in Figure 136. This is a vertical down borehole in the floor of the drift, and is in the same cross-section as boreholes 147, 148, and 149. Again, the predicted deformation lags the observations during the first 20 days of heating, after which the slopes are similar.

The basecase model is closer in magnitude to the observed deformation at MPBX 4 by about 0.3 mm (day 545) than the continuum model, and the deformation rate appears to be slowing in the data. This change in rate is not predicted by the model. The magnitude of the prediction at day 545 is well within 10% of the observed value (4.8 mm predicted by the basecase model vs. 5.0 mm observed).

Borehole 156: This is a vertical up borehole located in the middle fan of the MPBX boreholes shown in Figure 123. Observed and predicted deformations are shown in Figure 137. For this borehole, predictions show a small negative deformation for the first 100 days, while observations during this time show a rapid expansion. After 100 days the slope of the predicted deformation is very similar to that of the observed. At 545 days the estimate of 3.5 mm is within 20% of the 4.7 mm observed value.

Borehole 180: This is another vertical up-hole in the crown. Results of observations and predictions (Figure 138) are similar to those for boreholes 149 and 156. That is, the model shows low or negative expansion for the first 100 days and lags the observed deformation. The slope of the model and the observations after 100 days are very similar through 330 days. Observed deformation data are unavailable between 330 and 540 days. Data are available after 540 days, and the predicted value of 3.5 mm is within 10% of the observed value of 3.7 mm at 545 days. Continuum and basecase model predictions are very similar, as there are few fractures currently mapped in this region.

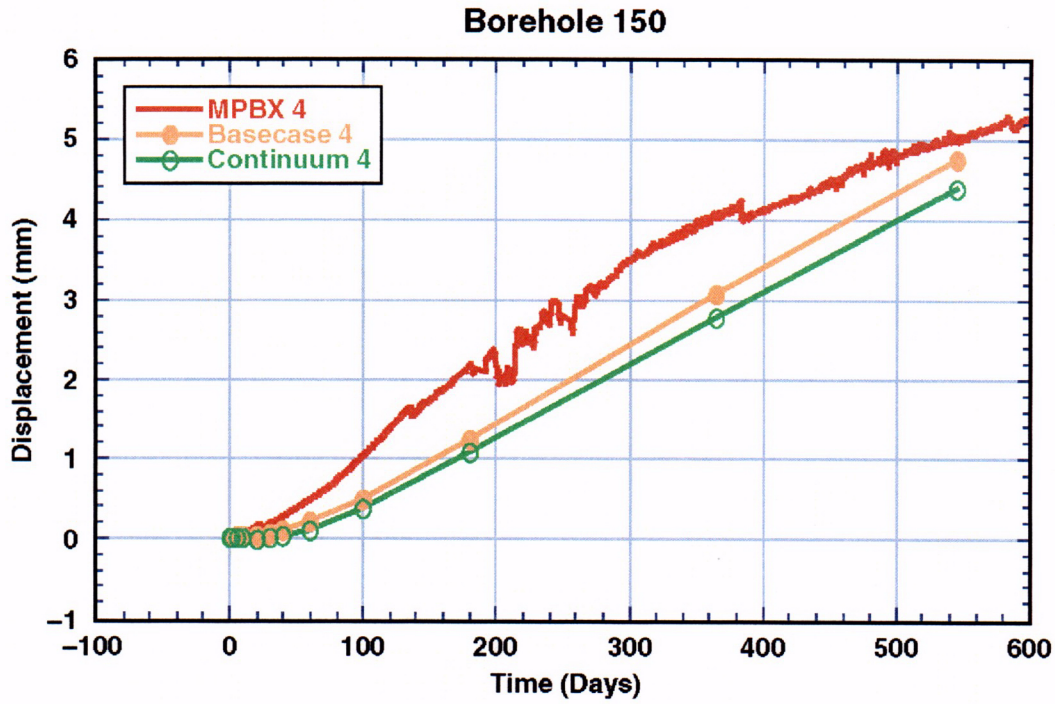

Figure 136. Observed and Predicted Deformation for BH 150.

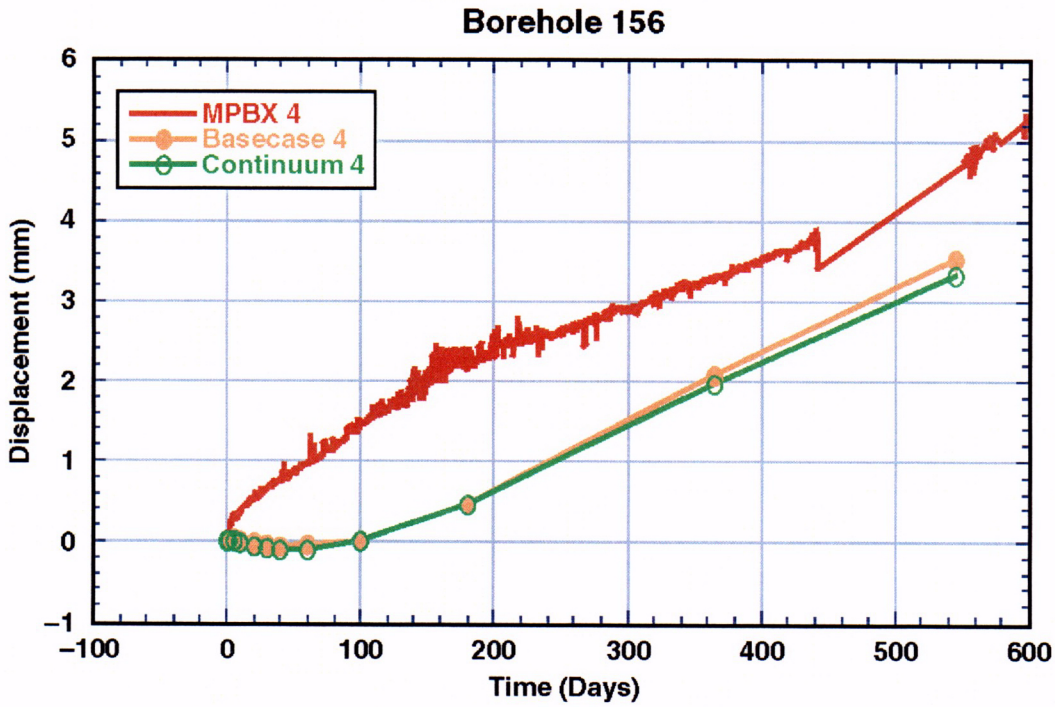

Figure 137. Observed and Predicted Deformation for BH 156.

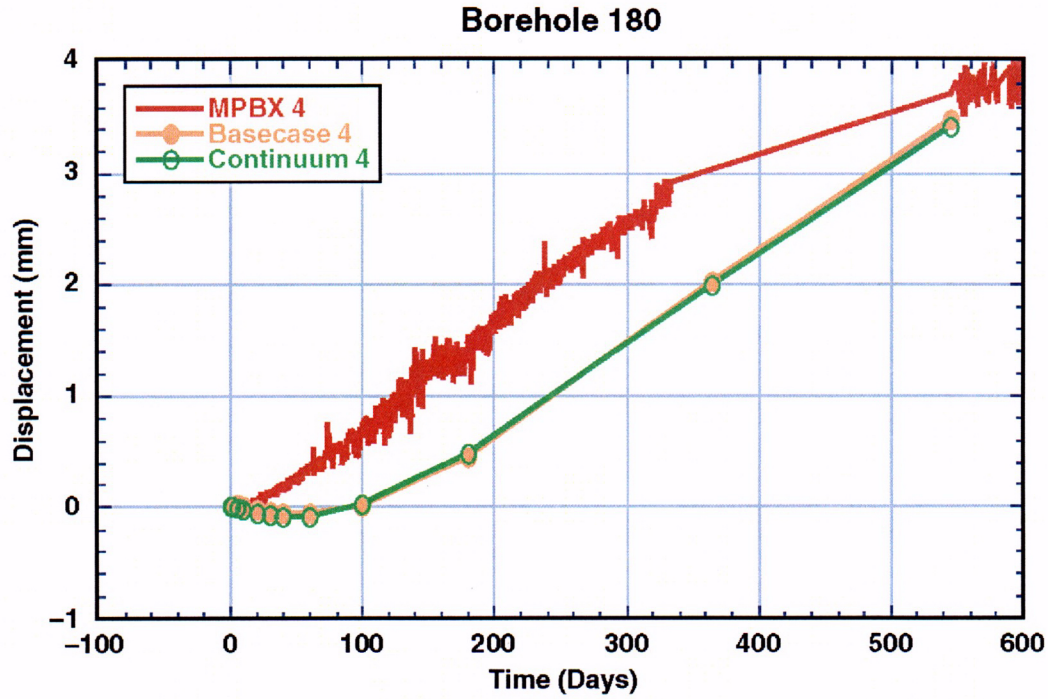

Figure 138. Observed and Predicted Deformation for BH 180.

Statistical Validation of THM Model. In addition to the qualitative comparison of predicted and observed deformation for the DST, three statistical measures were used to compare measured and simulated displacements. These measures are the root-mean-square difference (RMSD), the mean difference (MD), and the normalized-absolute-mean difference (NAMD). The application of these statistical measures provides a quantitative approach that complements the qualitative comparison of the predicted and measured deformations. These statistical measures are based on standard statistics (Bowker and Lieberman 1972) which have been modified to better adapt to interpretation of measured and simulated behavior in the thermal test.

The root-mean-square difference (RMSD) for a specific time after the start of heating is defined as:

$$RMSD = \left[\frac{\sum_{i=1}^{N} \left(d_{sim,i} - d_{meas,i} \right)^2}{N} \right]^{1/2}$$

where $d_{sim,i}$ and $d_{meas,i}$ are the simulated and measured displacements for the ith MPBX anchors. N is the number of anchors compared at a particular time. The anchors used in this analysis are listed in Table 8. The smaller the RMSD the better the agreement between simulated and measured displacements.

The mean difference (MD) for a specific time is defined as:

$$MD = \frac{\sum_{i=1}^{N} \left[d_{sim,\,i} - d_{meas,\,i} \right]}{N}$$

A positive MD indicates an overestimate or overprediction of displacements, whereas the converse applies for a negative MD.

The normalized absolute mean difference (NAMD) for a specific time is computed using:

$$NAMD = \sum_{i=1}^{N} \left| \frac{d_{sim,\,i} - d_{meas,\,i}}{d_{meas,\,i}} \right| * \frac{1}{N}$$

The NAMD provides a percentage of the absolute difference between measured and simulated displacement relative to the measured displacement.

Figure 139 shows the time history for each of the three statistical measures (RMSD, MD, and NAMD) used to assess the agreement between measured and calculated displacements for both the base case (discrete model) and the sensitivity case (continuum model).

The overall agreement is reasonable for this initial analysis of the mechanical behavior in the DST. Also, it appears that the two cases considered (discrete and continuum models) do not differ substantially in their ability to simulate the measured displacements. These findings will need to be updated in future statistical analyses that will involve a more robust comparative analysis by including substantially more MPBX anchors. The RMSD shown in Figure 139 shows a general linear increase after the initial 20 days of heating for both cases considered. The 500-day magnitudes are slightly less than 3 mm. Figure 139 shows that the MDs for both cases are also quite similar for the times considered. These MDs, which are averages of all MDs determined at a specific time, range from 0.0 mm to –0.5 mm over the initial 500 days of heating. Upon further examination of the MDs for individual anchor locations, the MD ranges from –4.5 mm to 2.5 mm. Consequently, the MDs in this analysis tend to offset each other, resulting in the trends shown in Figure 139. The NAMDs shown in the figure are as high as 250 percent during the initial 100 days of heating. Thereafter, they are better but still average approximately 150 percent over the next 400 days. Upon examination of individual MPBX boreholes/anchors, it becomes apparent that a few of the MPBX boreholes contribute to the substantially large NAMDs. In some instances, these large NAMDs reflect comparatively small measured displacements. This behavior is noticeably present in the long longitudinal MPBX boreholes (81 and 82) that are slightly above and outside the Heated Drift. This general and unfavorable trend suggests that modeling of the displacements parallel to the axis of the Heated Drift will need to be reevaluated including characterization of fractures or discontinuities.

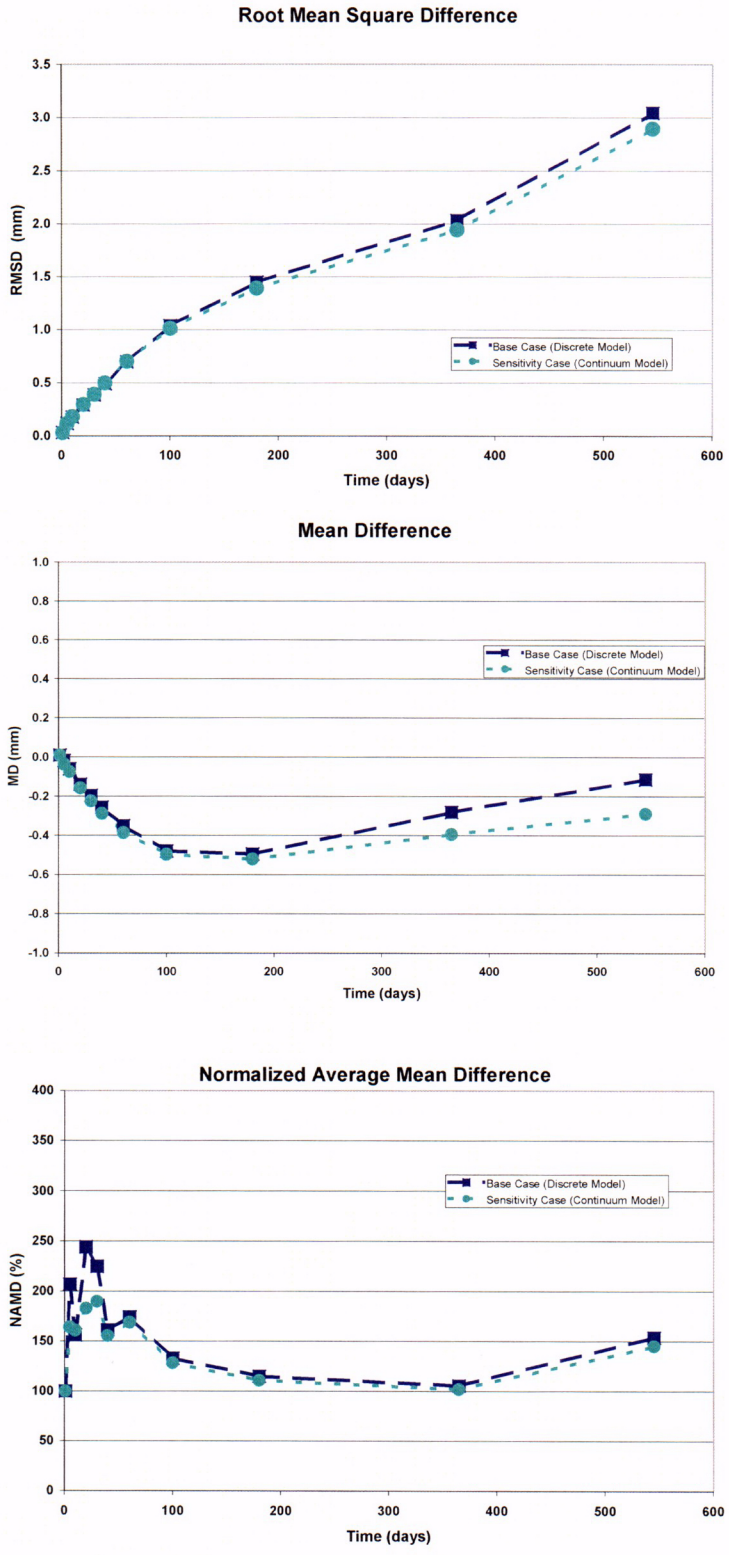

Figure 139. Statistical Measures for Comparative Analyses of Drift Scale Test Displacements.

5.3.2 Large Block Test

Test Description and Model Development
The Large Block Test (LBT) was conducted at Fran Ridge, near Yucca Mountain, Nevada, and comprised one phase of the field-scale thermal testing program of the Yucca Mountain Site Characterization Project. The particular objective of the LBT was to monitor and characterize coupled THMC processes in an isolated block of fractured rock subject to a one-dimensional thermal gradient (Wilder et al. 1997). Because the block is an unconfined and well-mapped fractured rock mass, it is a good candidate for analysis using discontinuum models.

The LBT was conducted on a rectangular prism of rock 3 m × 3 m in cross-section and 4.5 m high that was exposed from an outcrop by excavating the surrounding rock. Detailed geologic mapping showed that two subvertical sets of fractures and one set of subhorizontal fractures intersect the block. The subvertical fracture sets are approximately orthogonal, with spacings of 0.25 to 1 m and are oriented generally in the NE–SW and NW–SE directions. Moreover, a major sub-horizontal fracture is located approximately 0.5 m below the top surface.

To create a one-dimensional thermal field within the block, heaters were placed in the rock to simulate a plane heat source at a height of 1.75 m from the base of the block, and a steel plate fitted with heating/cooling coils was mounted on the top of the block. This plate was connected to a heat exchanger to allow thermal control of the top surface. The block was heated for more than 12 months, from Feb. 27, 1997, until March 10, 1998.
The overall three-dimensional mechanical response of the rock to the heating was monitored using six multiple-point borehole extensometers (MPBXs). Three were oriented horizontally in the N–S direction; two were oriented horizontally in the E–W direction, and one was oriented vertically. The geometry of the heaters, MPBX boreholes, and one temperature borehole is shown in Figure 140.

A THM model for the LBT has been formulated using the general approach presented above. This model incorporated the general geometry of the LBT. Data for the simulations is given in Tables 4, 6, and 7. The input and output files for the Large Block Test model validation simulations have been submitted to the TDMS (DTN: LL010703623123.01).

Temperatures. Deformation of the LBT was calculated at times of 0, 10, 25, 55, 85, 115, 145, 182, 200, 275, 340, 350, 375, 385, 395, 410, 430, and 450 days after the start of heating. The temperatures in this analysis were derived from the TH analysis reported in CRWMS 2000, Section 6. Files containing Cartesian coordinates and temperatures for the model region simulated by NUFT were obtained at each time. The NUFT model assumes symmetry in the block; consequently these files contained values for one quadrant of the region simulated in 3DEC. The 3DEC calculations include the entire volume of the block, as the fractures are not symmetric. A 3-dimensional temperature field for 3DEC was produced from the NUFT temperatures by reflecting the temperatures about the appropriate vertical planes. This was done as follows. Temperatures from the NUFT model and their coordinates were input into EarthVision along with an array of

grid points generated by 3DEC for the LBT model domain at each calculation time. EarthVision performed a three-dimensional interpolation of the 3D NUFT model temperatures to provide an interpolated temperature for each calculation time at each of the 3DEC model grid points. The grid point temperatures were then input into 3DEC as a separate input file for each calculation time.

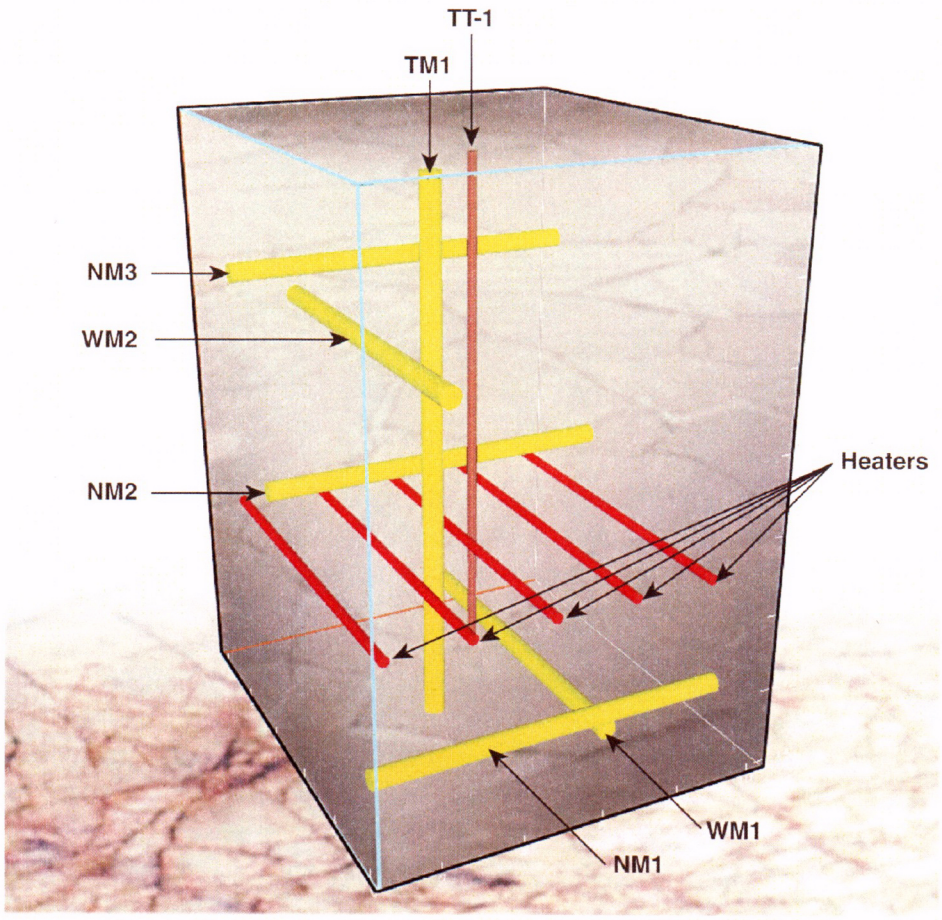

Figure 140. MPBX Borehole Locations in the Large Block Test.

Fractures. Fractures used in the simulations were taken from the LBT fracture data set described in Wilder et al. (1997, Section 2.2). Particular fractures used in the simulations are discussed below. The fractures were assumed to have no tensile strength.

Model Geometry. The spatial domain for the LBT model is shown in Figure 141, top left. This model domain extends 23 m beneath the ground surface and 23 m out from each vertical face of the LBT, so that the fixed displacement boundary conditions can be applied far from the heated portion of the block. At these distances thermal expansion cannot reasonably be expected, so that fixed displacement boundary conditions may be applied with confidence.

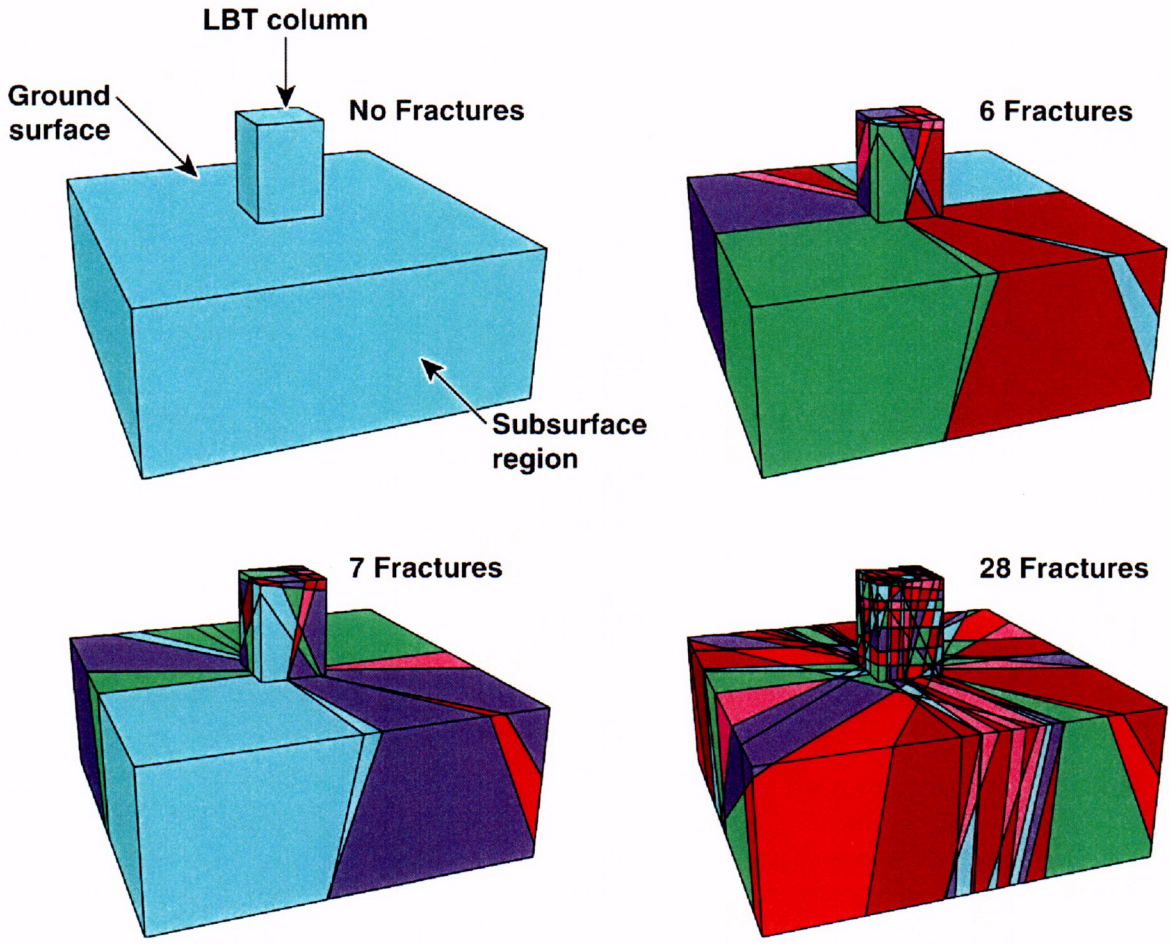

Figure 141. Spatial Domain for the Model.

Boundary Conditions. Roller boundary conditions were imposed on the four vertical sides and on the base of the subsurface region. These boundary conditions impose a zero displacement restriction on normal displacements along these surfaces, but allow parallel (in plane) displacements. Thus, horizontal displacements are permitted along the base of the block and vertical displacements are permitted along the sides of the subsurface region. Fixed displacement boundary conditions provide an upper bound on thermal stresses because outward displacements of the model sides, which would relieve built-up stresses, are not allowed.

The base of the block was fixed in the vertical direction to prevent the rock at 23 m below the LBT from moving vertically. The top of the block is allowed to move vertically. This is appropriate because the LBT column is unconfined, whereas the base of the model is supported by the underlying rock. A fixed stress boundary condition, equal to atmospheric pressure, is applied to the top and sides of the LBT columnar region and to the ground surface region in the model.

C-89

Rock Properties. Input parameters for the LBT simulation are provided in Table 6. Calculated or assumed parameters are listed in Table 7.

Simulations. A series of simulations (referred to as "Models" in the following discussion) were conducted to evaluate the effect of number of fractures and of Coefficient of Thermal Expansion (CTE) on the mechanical behavior. The simulations are listed in Table 10 and the fracture geometries of the model domain for the various simulations are shown in Figure 141.

Table 10. Summary of THM Simulations of the LBT

Model #	Number of Fractures	CTE ($\times 10^{-6}$/°C)	Comment
1	0	5.27	Continuum model
2	6	9.73	High CTE with 6 major fractures
3	6	5.27	Low CTE with 6 major fractures
4	7	5.27	Same as 3 with one additional fracture
5	28	5.27	All fractures included in fracture analysis

Results for Large Block Test

The 3DEC model was configured to produce displacement values at the locations of the MPBX anchors discussed above. Deformation in the vertical direction was monitored in borehole TM1, and predicted displacement is compared with observed displacement for anchor TM1-4 in Figure 142a for the first 100 days of heating. This figure plots results for each simulation along with the observed displacement and shows that while Model 2 with high CTE matches the early thermal deformation up to 20 days, it overpredicts the deformation at 100 days by more that a factor of 2. Predictions produced by the other four models, with lower CTE, are quite acceptable as they underpredict the magnitude of the displacement by only a few tenths of a millimeter. The continuum and fractured models produce similar estimates, and the response of all of these models lags the observed deformation during the first 40 days. Thus, the number of fractures had very little effect on predicted deformation for the vertical direction.

Predicted deformation during cooldown is compared with field measurement at anchor TM1-4 in Figure 142b. This plot shows that the continuum model (Model 1) fits both the shape and magnitude of the observations, while Model 3 with six fractures also approximates the observations quite well.

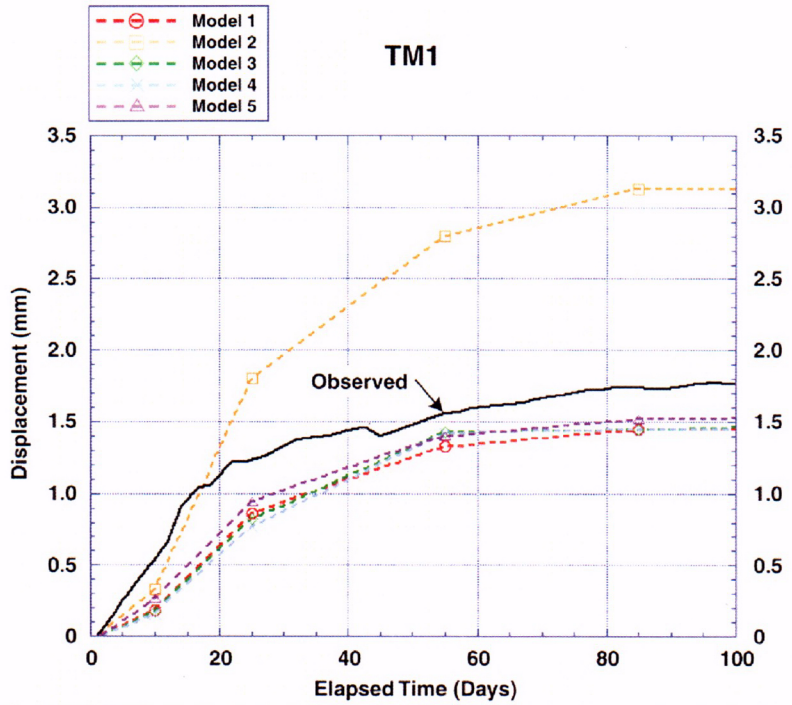

Figure 142a. Simulated Deformation in the Vertical Direction Compared with Field Measurements for Anchor TM1-4.

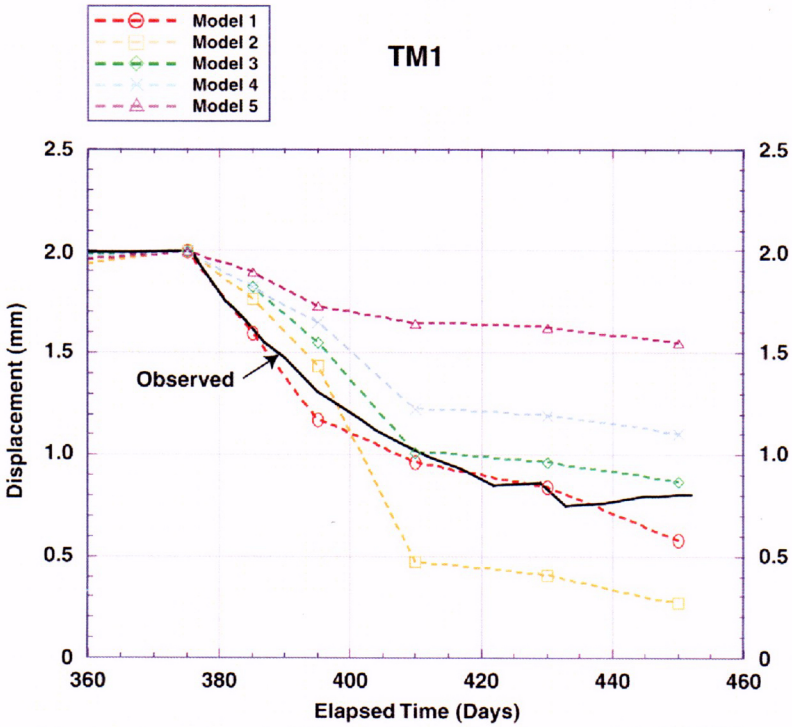

Figure 142b. Simulated Deformation during Cooldown Compared with Field Measurement at Anchor TM1-4.

MPBX boreholes NM1 and WM1 were located close to the bottom of the block and in orthogonal directions. Measured and predicted displacement values for anchor NM1-4 are plotted in Figure 143a. This figure shows that at this location, Model 3 provides the best match to the observations. Model 2 overpredicts displacement by nearly a factor of 2, while the continuum model (Model 1) underpredicts the deformation. Models 1, 3, 4, and 5 bracket the observed values, with Model 1 underpredicting for the first 100 days and Models 4 and 5 overpredicting at 100 days. This plot indicates that while Model 3 (6 fractures) slightly underpredicts deformation, adding one fracture (Model 4) caused more displacement at this location, but adding many fractures (Model 5) caused underprediction during the first 25 days and overprediction after 25 days.

Results for NM1-4 during cooldown are shown in Figure 143b. This figure shows that at this location Model 3 matches the magnitude of the displacement, but does not accurately predict the cooling path. Model 2 overpredicts the displacement and best approximates the slope of the curve during the first 20 days of cooling. Models 1, 4, and 5 underpredict the amount of recovery during cooldown. The least contraction is predicted by Model 5, the highly fractured rockmass.

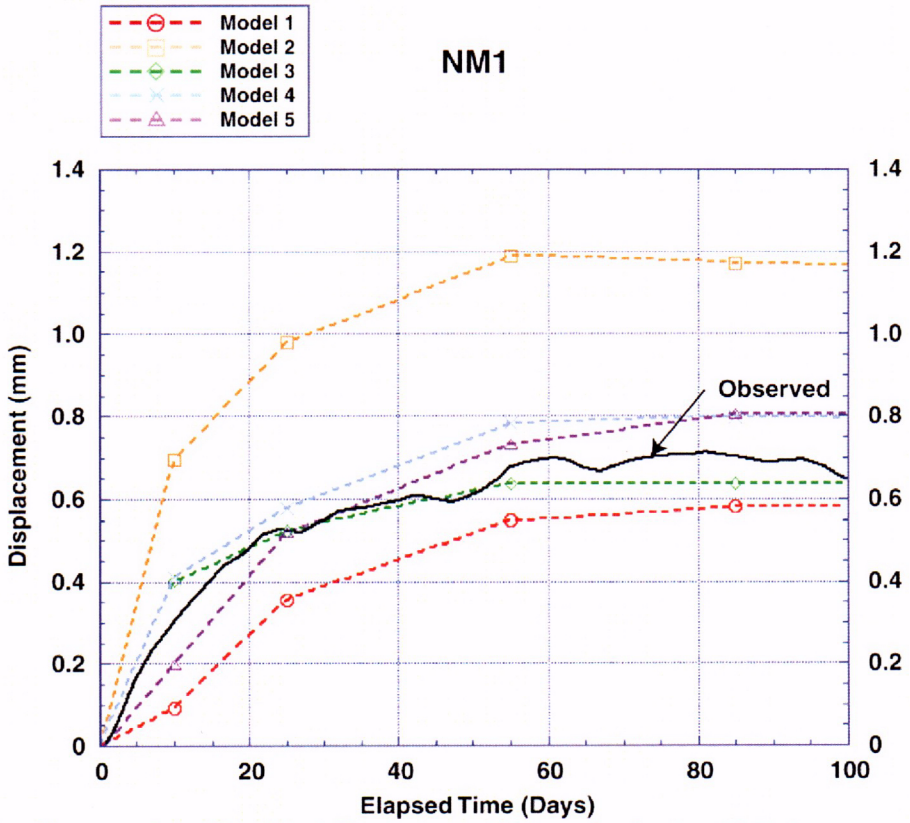

Figure 143a. Measured and Predicted Displacement Values for Anchor NM1-4.

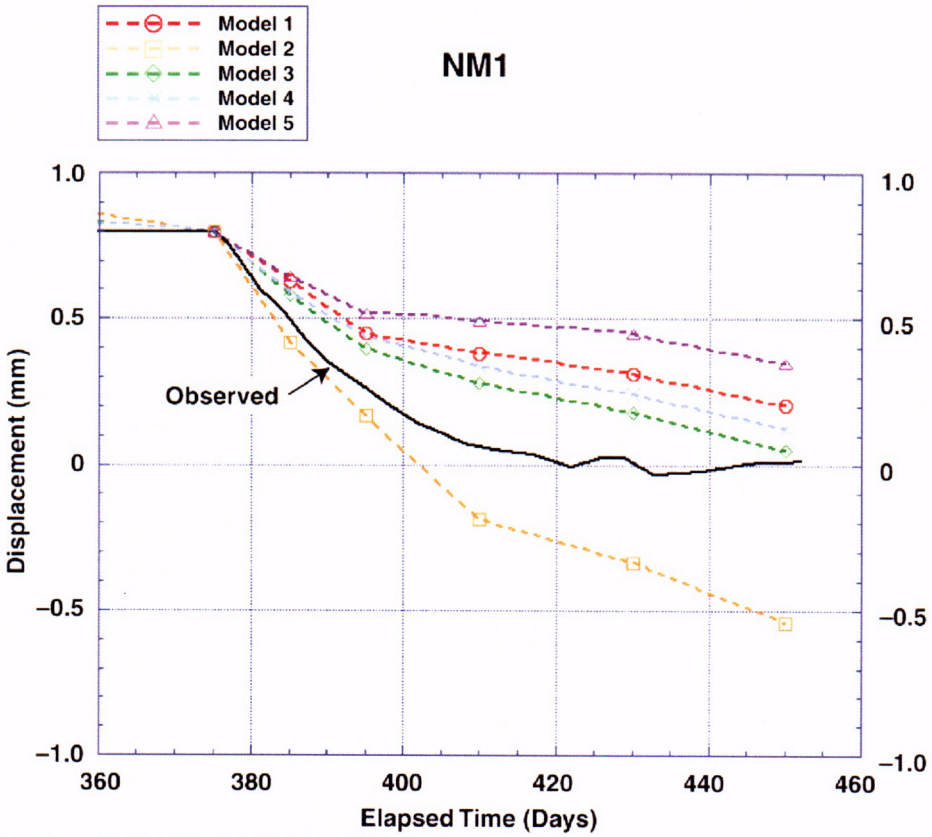

Figure143b. Results for NM1-4 During Cooldown.

Data and predictions for the first 100 days of heating for WM1 are shown in Figure 144a. This plot shows similar results to Figure 143a in that Model 2 overpredicts by nearly a factor of two, and models 1, 3, 4, and 5 bracket the behavior. The highly fractured model (Model 5) best approximates the response during the first 20 days; Models 3 and 4 overpredict the displacement during the first 10 days, but are within about 0.05 mm of the observed displacement at 100 days. Model 1 underpredicts the displacement by between 0.1 and 0.15 mm throughout this time interval.

Modeling results for WM1 during the cooldown period are shown in Figure 144b. These results are similar to the results for NM1 in that the continuum model (Model 1) most closely approximates the observed cooldown. The high CTE model (Model 2) overpredicts the deformation, while the other models underpredict the displacement. Interestingly, these results show that adding fractures to the model causes less recovery during cooldown. This may be because fracture slip is essentially unrecoverable under unconfined stress conditions.

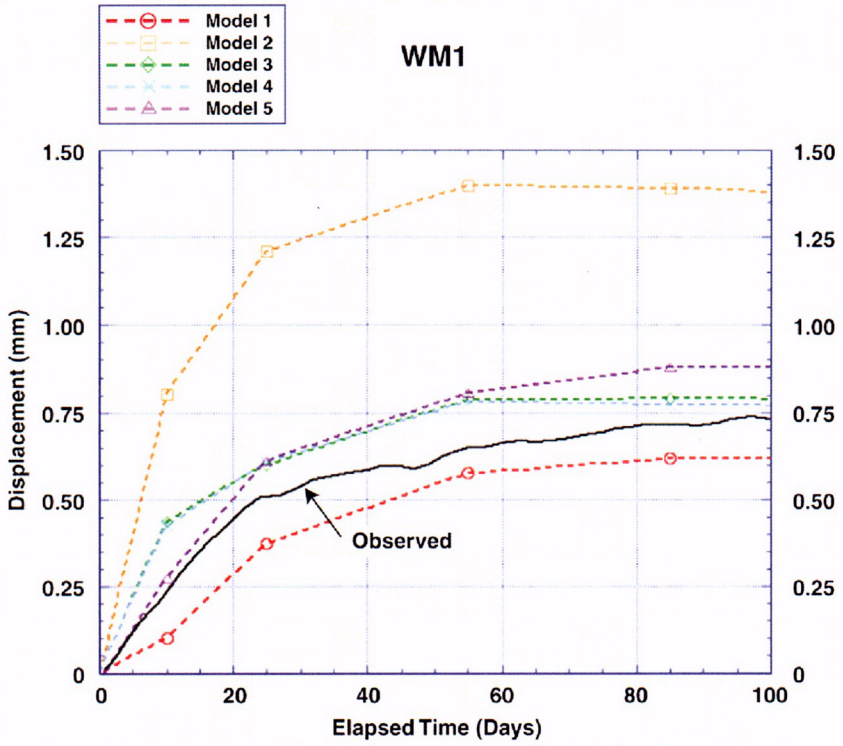

Figure 144a. Data and Predictions for the First 100 Days of Heating for WM1.

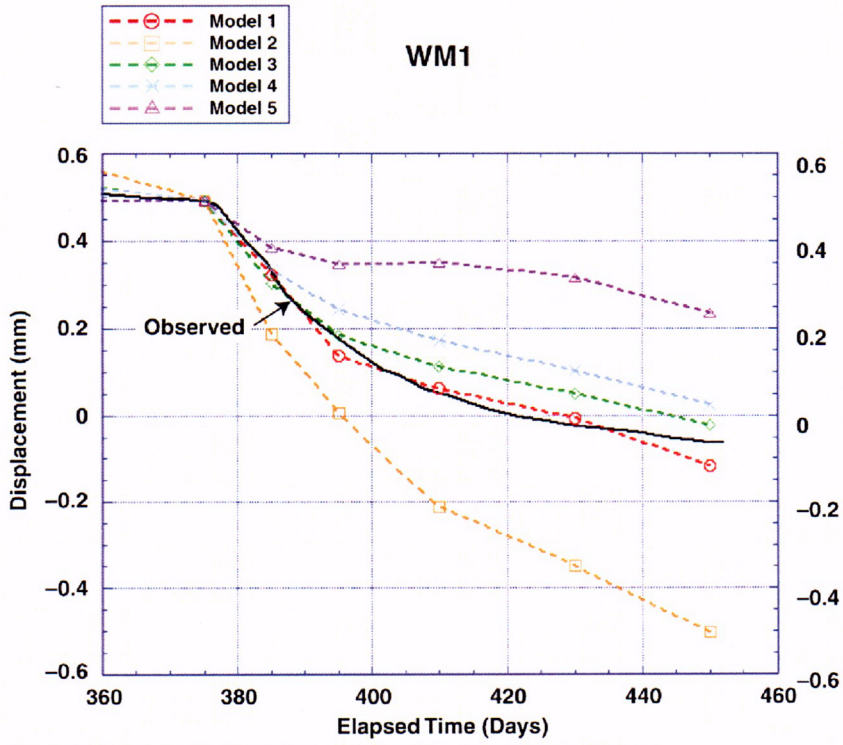

Figure 144b. Modeling Results for WM1 During the Cooldown Period.

C-93

Figure 145 presents simulated and observed displacements for borehole NM2, which was located near the heater plane. This figure shows that the continuum model (Model 1) underpredicts the displacement for anchor NM2-4, while the high CTE model (Model 2) predicts the deformation relatively well during the first 10 days, but overpredicts the magnitude of the total deformation at 40 days by nearly a factor of 2. Models 3, 4, and 5 produce similar results, and both Models 4 and 5 cross over the observed deformation at 40 days. Of these three models, Model 5 provides the best fit to the data for the first 40 days, indicating that rock in this region is highly fractured.

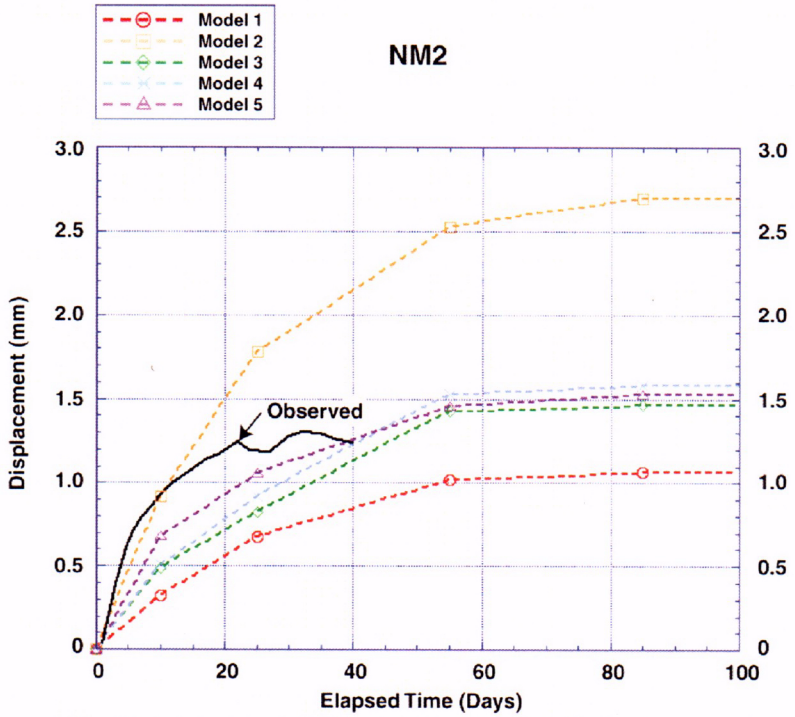

Figure 145. Simulated and Observed Displacements for Borehole NM2.

The MPBX instrumentation in borehole WM2 functioned throughout the test and data for anchor WM2-4 for the entire test is shown along with simulated displacements in Figure 146. This figure shows that for this anchor, Models 3 and 4 did a good job of predicting the deformation over much of the test duration. Model 3 predicts slightly less displacement than Model 4, and from 50 to 100 days Model 4 is closer to the observations, while from 120 to 220 days Model 3 fits slightly better. Models 3 and 4 also capture the cooldown relatively well. They underpredict the total amount of cooldown displacement, by 0.4 mm, and also show some contraction of the block about 270 days that is not reflected by the observation. Models 1 and 5 both underpredict maximum deformation by significant amounts (1.6 and 1 mm respectively). Model 2 overpredicts the maximum deformation, but does show the best fit to displacement during the first 20 days of heating. Model 5 does not show contraction with cooldown and Model 1 underpredicts the magnitude of the cooldown displacement. Model 2 correctly predicts the relative change in displacement during cooldown (1.8 mm) but the final value of 2.6 mm displacement is too high.

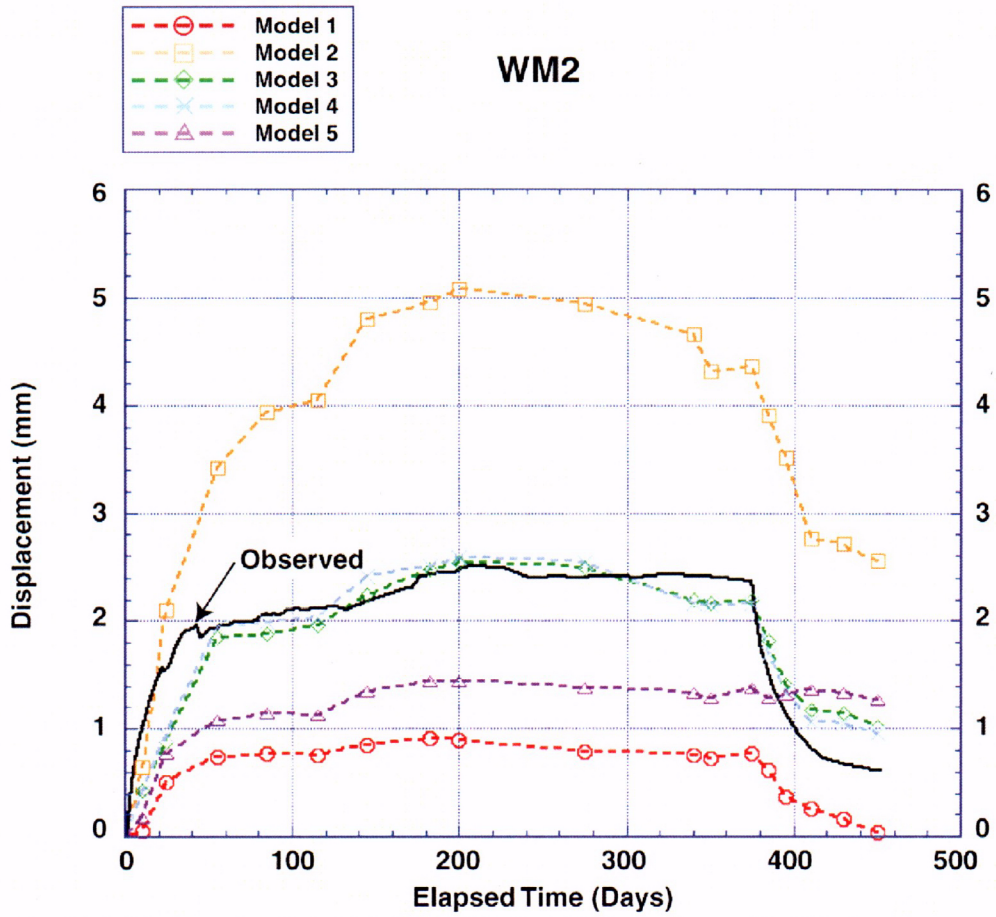

Figure 146. Data for Anchor WM2-4 for the Entire Test Shown Along with Simulated Displacements.

Continuous data are also available for anchor 4 of borehole NM3, the uppermost horizontal MPBX borehole in the block, and these data are shown with the model predictions in Figure 147. While the measured NM3-4 displacements are similar to those for WM2-4, with a maximum displacement between 2.5 and 3 mm, all of the models underpredict the measured NM3-4 displacements. This result differs considerably from that of the other MPBX boreholes. Adding one fracture to Model 3 to create Model 4 did increase the predicted NM3-4 displacements, but the increase was only a small fraction of that needed to compare well with the observations.

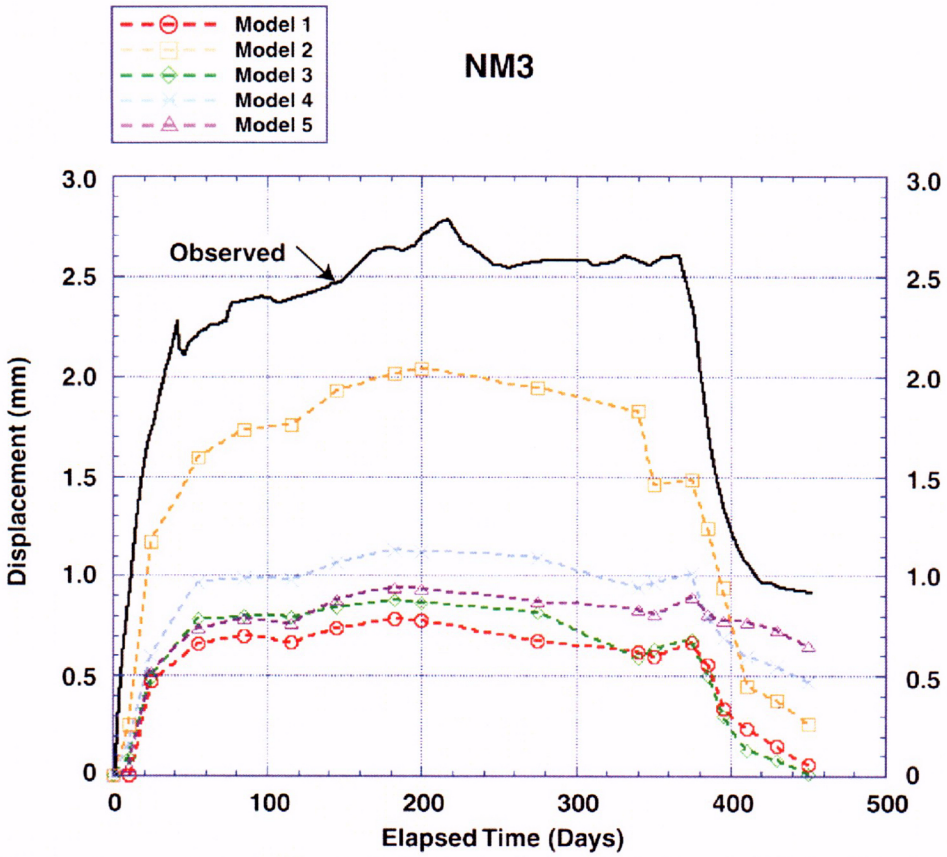

Figure 147. Continuous Data for Borehole NM3, Anchor NM3-4, Shown with the Model Predictions.

The results discussed above indicate that Models 3 and 4 provide the best overall fit to the observations. Model 1 fits the results at the bottom of the block relatively well.

The difference between the measured and predicted deformation during the first 50 days of heating is of interest as it relates to the transient response of the rock to the temperature field. Figures 143a and 144a show that for horizontal boreholes near the base of the block, deformation in Models 3 and 4 lead the observed displacements during the first 20 days. Figures 145 and 146 show that the observed deformation leads the predictions during the first 40 to 60 days of heating. Predicted and observed results for anchor WM2-4 for the first 100 days of heating are replotted in Figure 148 along with temperature data for the plane of the heater and the plane of WM2, respectively. This figure shows that during the first 30 days the observed deformation (WM2-4) can be correlated with temperature at the heaters (TT1-14), while the predicted deformation is correlated with temperature at the borehole location (TT1-22). This indicates that movement of the rock above the heater may be due to a far-field effect, and may imply that movement along fractures serves to propagate deformation.

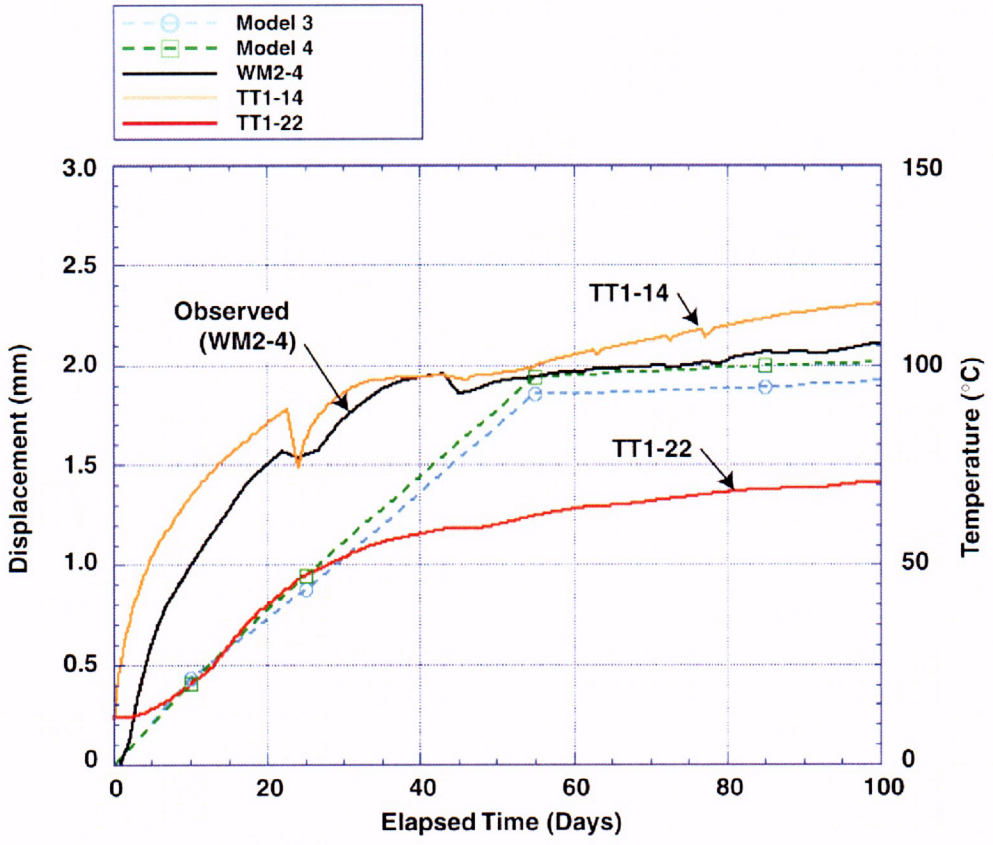

Figure 148. Predicted (Model 3, Model 4) and Observed (WM2-4) Displacements for Anchor WM2-4 during the First 100 days of Heating along with Temperatures for the Heater (TT1-14) and WM2 (TT1-22) Planes.

5.3.3 Conclusions

A coupled THM model has been formulated for analysis of TM behavior in fractured rock at Yucca Mountain. This model uses temperature computed by the NUFT TH code as input to the 3DEC distinct element mechanical code. The model has been used to simulate both the DST and the LBT. Predictions of deformation for these two tests have been made using the model in both a continuum mode and in formulations containing discrete fractures. Comparison of the predicted deformation with observations made using MPBX instrumentation shows that generally the predictions capture both the trend and the magnitude of the observations. Moreover, for both the DST and the LBT, the simulations containing discrete fractures more accurately predict the deformation behavior than do simulations with no fractures. This work indicates that not all fractures are active in the tests, and for the LBT, the deformation was controlled by a subset of 6-10 major fractures.

Results show that a CTE value of 5.27e-6/°C is appropriate for the LBT. This is consistent with the value determined for the Single Heater Test. However, a higher value of 9.73e-6/°C provided a good fit to deformation in the DST.

The transient response of the predicted deformation at early times lags the observed deformation in both tests. This is caused in part by the lag in predicted temperatures when compared to observed temperatures. The TH thermal models must be improved in early times in order to correctly predict the TM behavior.

5.3.4 References

Bowker, A.H. and Lieberman, G.J. 1972. *Engineering Statistics.* 2nd Edition. Engelwood Cliffs, New Jersey: Prentice-Hall, Inc. TIC: 240460.

CRWMS M&O 1997. *Drift Scale Test Design and Forecast Results.* BAB000000-01717-4600-00007 REV 01. Las Vegas, Nevada: CRWMS M&O. ACC: MOL.19980710.0155.

CRWMS M&O 1998. *Drift Scale Test As-Built Report.* BAB000000-01717-5700-00003 REV 01. Las Vegas, Nevada: CRWMS M&O. ACC: MOL19990107.0223.

CRWMS M&O 2000. *Thermal Tests Thermal-Hydrological Analysis/Model Report.* ANL-NBS-TH-000001 REV 00. Las Vegas, Nevada: CRWMS M&O. ACC: MOL.20000505.0231.

CRWMS M&O 2001. *Coupled Thermal-Hydrologic-Mechanical Effects on Permeability Analysis and Models Report.* ANL-NBS-HS-000037 REV 00. Las Vegas, Nevada: CRWMS M&O.

Itasca Consulting Group, Inc. 1998. *3DECV2.0.* V2.0. STN:10025-2.0-00.

Jaeger, J.C. and Cook, N.G.W. 1979. *Fundamentals of Rock Mechanics.* 3rd Edition. New York, New York: Chapman and Hall. TIC: 218325.

Schelling, F.J. 1989. *DR22-B-In Situ Stress Near ESF.* Albuquerque, NM: Sandia National Laboratories. ACC: NNA.19890523.0038.

Wilder, D.G.; Lin, W.; Blair, S.C.; Guscheck, T.; Carlson, R.C.; Lee, K.; Meike, A.; Ramirez, A.; Wagoner, J.L.; and Wang, J. 1997. *Large Block Test Status Report,* UCRL-ID-128776. Livermore, California: Lawrence Livermore National Laboratory. ACC: MOL.19980508.0727.

5.4 Acoustic Emission/Microseismic Monitoring:

From October, 2000 to June, 2001, no acoustic emission events have occurred. In fact, the last microseism was recorded on July 2, 2000 even though the system has been running continuously since then. Figure 149 shows a bargraph of microseisms per week for the total time the system was operating is shown below. The gap in August, 1999 was due to a power failure cause by a lightning storm which, coincidentally, was also during the time of high seismicity.

The hammer calibration test indicates that energy from the hammer blow can still be detected in the array, but at lower amplitudes for some stations. This suggests that drop off in seismicity is most likely real and not caused by a deterioration in station response, though some smaller events may be undetected due to attenuation of waves caused by the heated rock and/or high temperatures damaging the sensors. The seismicity plots remain the same as August, 2000 (Figures 150-2), since no events have been recorded since then.

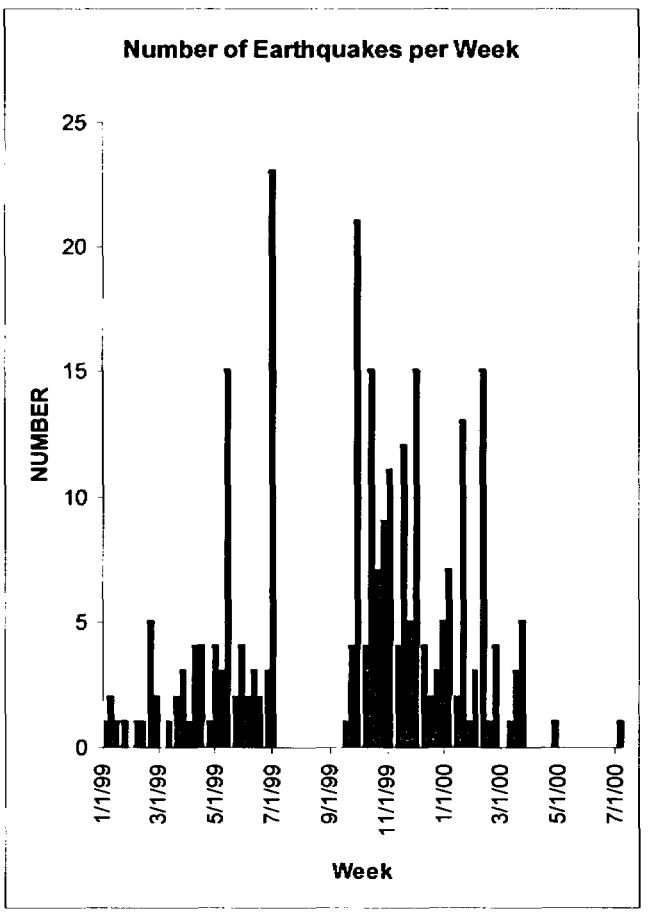

Figure 149. Graph of number of microseisms per week. No events recorded after July, 2000.

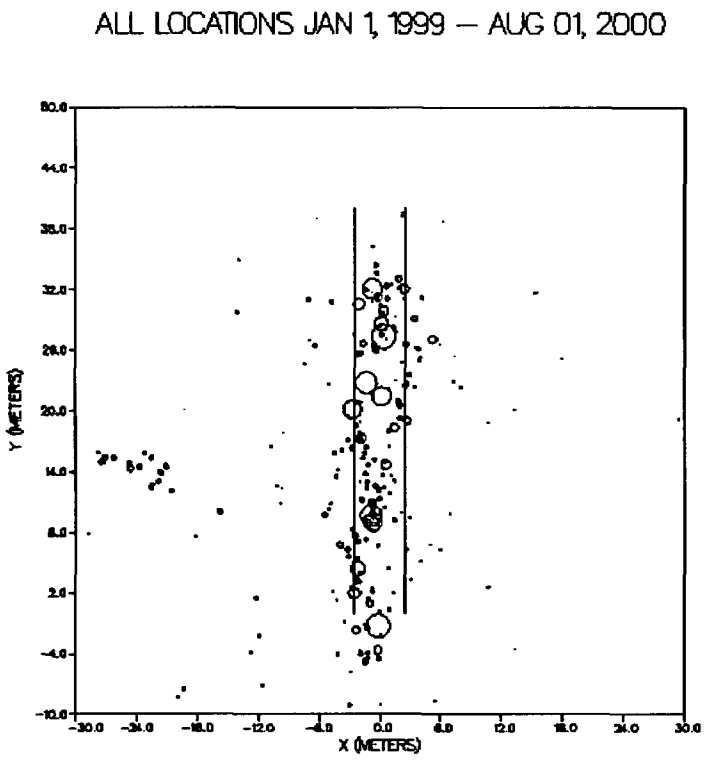

Figure 150. Plan view of microseismicity. The size of the circle indicates that relative magnitude of the microseismic event.

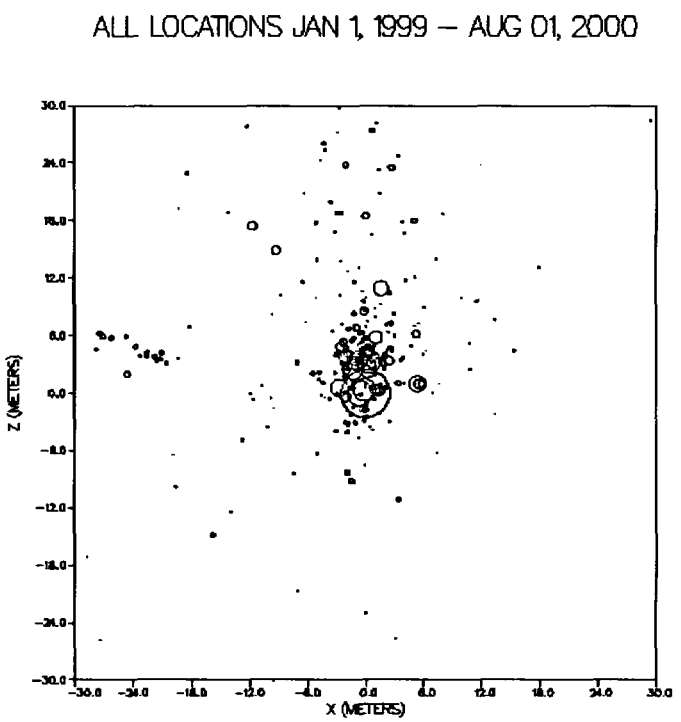

Figure 151. Same as Figure 150 with the events now projected onto the x-z plane. The largest circle at (0,0) represents the Drift.

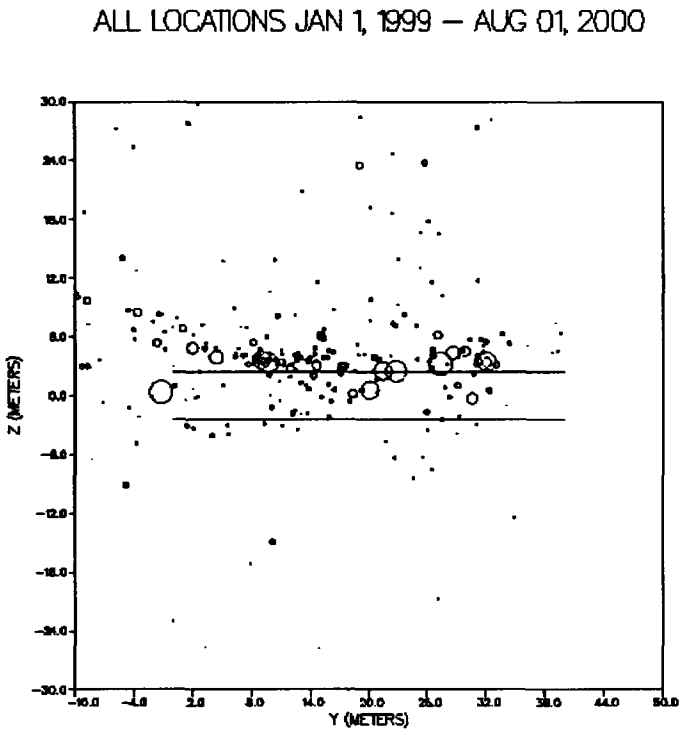

Figure 152. Same as Figure 150 with the events now projected onto the y-z plane.

INTENTIONALLY LEFT BLANK